NANO LETTERS

pubs.acs.org/NanoLett

Letter

High Osmotic Power Generation via Nanopore Arrays in Hybrid Hexagonal Boron Nitride/Silicon Nitride Membranes

Khadija Yazda, Katarina Bleau, Yuning Zhang, Xavier Capaldi, Thomas St-Denis, Peter Grutter,* and Walter W. Reisner*

Cite This: *Nano Lett.* 2021, 21, 4152–4159

Read Online

ACCESS | Metrics & More | Article Recommendations | Supporting Information

ABSTRACT: Nanopores embedded in two-dimensional (2D) nanomaterials are a promising emerging technology for osmotic power generation. Here, coupling our new AFM-based pore fabrication approach, tip-controlled local breakdown (TCLB), with a hybrid membrane formed by coating silicon nitride (SiN) with hexagonal boron nitride (hBN), we show that high osmotic power density can be obtained in systems that do not possess the thinness of atomic monolayers. In our approach, the high osmotic performance arises from charge separation induced by the highly charged hBN surface rather than charge on the inner pore wall. Moreover, exploiting TCLB's capability of producing sub 10 nm pore arrays, we investigate the effects of pore−pore interaction on the overall power density. We find that an optimum pore-to-pore spacing of ∼500 nm is required to maintain an efficient selective transport mechanism.

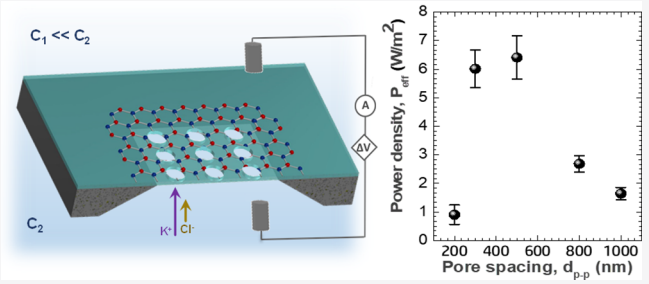

KEYWORDS: *Nanopores, two-dimensional nanomaterials, osmotic power generation, ion transport, pore−pore cross talk*

Downloaded via MCGILL UNIV on May 27, 2021 at 15:47:53 (UTC).
See https://pubs.acs.org/sharingguidelines for options on how to legitimately share published articles.

INTRODUCTION

There is growing need to provide local, inexpensive, and environmentally friendly power sources for a wide range of miniaturized electronic devices, for example implantable devices for medical monitoring, nano/micro-electromechanical systems and wireless sensor networks (WSN) for environmental monitoring.[1−3] These systems usually operate on a low power level ranging from nanowatts to microwatts. If power could be extracted directly from the local environment, rather than through a battery, this would lead to considerable cost savings and greater sustainability by eliminating the need for battery replacement and/or recharging from a centralized power source. To this end, considerable effort has been devoted to the development of technologies for converting renewable energy sources in the environment, such as mechanical vibrations[4−6] or waste heat,[7] into electrical power.

Another notable renewable energy source that can be used for nano/micro-power generators is osmotic energy or salinity gradient energy.[8,9] Osmotic energy is the energy obtained by exploiting the free energy released when solutions of different salinities are mixed.[10] It is clean and sustainable and does not discharge carbon dioxide or thermal pollutants during operation. Osmotic energy can be exploited whenever sources of fresh and salt water are in proximity, such as captured rainwater over the ocean or near briny industrial effluents. Osmotic energy can be harvested using a membrane-based separation process via two main approaches: pressure retarded osmosis (PRO) and reverse electrodialysis (RED).[11−13] In reverse electrodialysis, ions are driven through cation- and anion-exchange membranes. Like dialytic batteries, a net electrical current can then be captured directly at the electrodes due to charge separation induced by the selective ionic flow through ion-exchange membranes. When considering reverse electrodialysis, membranes with excellent cationic/anionic selectivity, low resistivity, good mechanical stability, and antifouling properties are required for their practical usability and potential scalability. Most of the research in osmotic energy has focused on the development of nanoporous membranes from various advanced materials, including polymers[14−16] and ceramics,[8,17−21] because of their mechanical stability and rich chemistry that enables unique ionic selectivity tuning. However, the thickness of these materials (≥500 nm) lowers the osmotic conductance, and lack of precision over the pore size distribution limits the obtainable power density.

A proof-of-concept of single nanochannel osmotic energy conversion system was first reported by Guo et al.[9] using a single track-etched nanopore on polyimide, with a maximum estimated power density up to 3−260 mW·cm^{-2} by exploiting parallelization with a pore density of 10^8−10^{10} cm^{-2}. Recently,

Received: November 27, 2020
Revised: May 7, 2021
Published: May 13, 2021

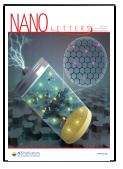

© 2021 American Chemical Society

https://doi.org/10.1021/acs.nanolett.0c04704
Nano Lett. 2021, 21, 4152−4159

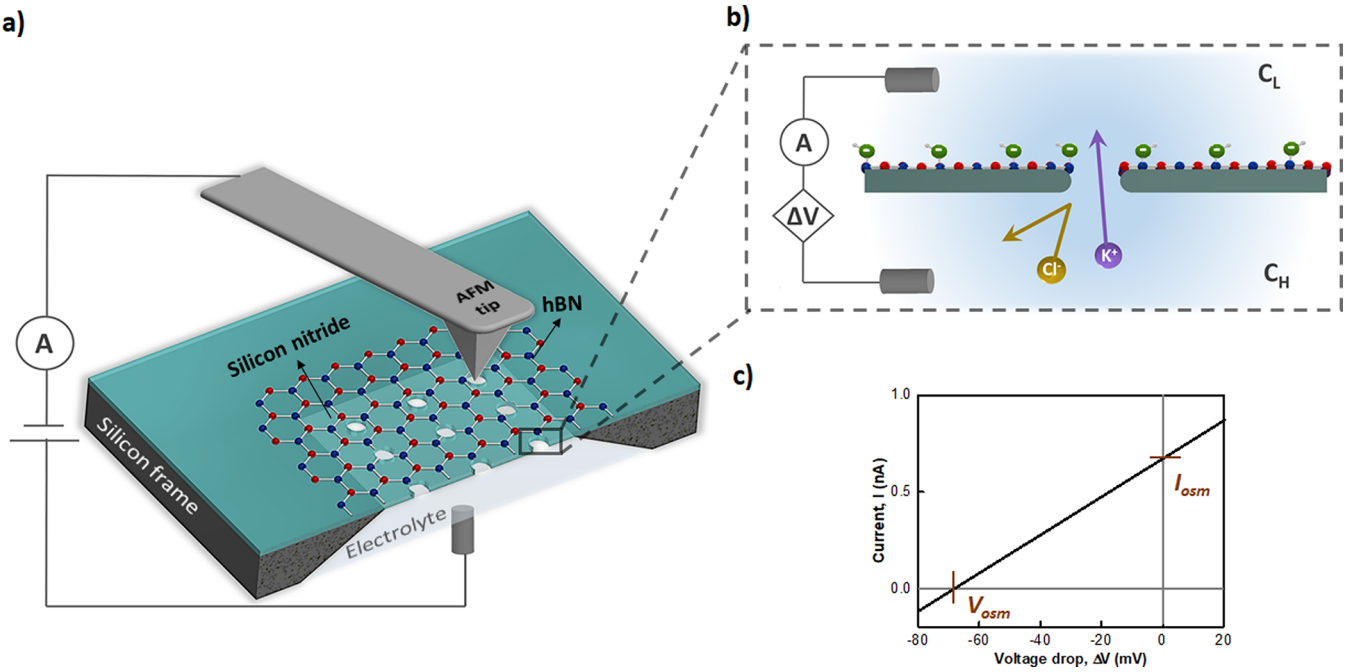

Figure 1. Hybrid hBN/SiN membrane setup for osmotic power generation: (a) The tip-controlled local breakdown technique (TCLB) is used to fabricate nanoporous arrays in a silicon nitride membrane (SiN_x) covered with a transferred boron nitride monolayer (hBN, boron atoms are blue spheres, and nitrogen atoms are red spheres). In TCLB, a conductive AFM tip positioned over the hBN/SiN membrane applies a voltage pulse leading to the formation of a nanopore at the tip position. Nanopore arrays with precise pore-to-pore spacing can be readily formed by controlling the tip position. (b) Ionic transport occurs through a single hBN/SiN nanopore separating two fluid reservoirs with differing potassium chloride (KCl) concentrations (C_H is the KCl concentration of the high salt reservoir, and C_L is the KCl concentration of the low salt reservoir). Selective cation transport (potassium ion, K^+) is observed because of the electrostatic screening by the hydroxide ions (HO^-) adsorbed at the boron atoms on the hBN side (O: green spheres, H: white spheres). (c) Current−voltage characteristics in a KCl concentration gradient and pH = 6 for a 6 nm single hBN/SiN nanopore. The pure osmotic behavior of the nanopore is obtained from the $I-V$ curve; the osmotic current (I_{osm}) and the osmotic potential (V_{osm}) are the nonzero y-intercept and x-intercept, respectively. The maximal osmotic power density extracted from the membrane is $P_{max} = \frac{1}{4} I_{osm} V_{osm}$.

nanomaterials such as nanotubes,[22,23] layered flakes,[24−26] and atomically thin suspended membranes[27−30] show exceptional promise for nanofluidic osmotic power generation.[31] Siria et al.[23] reported a record high value of 4 kWm^{-2} (per pore area) using a boron nitride nanotube (BNNT) of 15−40 nm diameter embedded in silicon nitride membrane. This high-power density was attributed to a diffusio-osmotic fluid flow transport originating from the high surface charge carried by the nanotube's internal surface. Later, Feng et al.[28] reported a 3 orders of magnitude enhancement in power density (1 MWm^{-2} estimated considering 30% porosity) using single nanopore embedded in ultrathin monolayer molybdenum disulfide (MoS_2) membranes. The extraordinary selectivity-permeability combination found in thin nanomaterials makes them promising candidates for osmotic energy conversion.

Yet, scaling thin membranes approaches is extremely challenging because of the difficulty of producing mechanically stable monolayer membranes.[32] Another challenge is the difficulty in scaling technology demonstrations performed with sufficiently small single pores to multipore arrays. Dielectric breakdown approaches create small pores but only at a random location on a membrane.[33,34] While arrays of sufficiently small pores can be produced with approaches based on high-energy beams, such as TEM and helium (He) ion microscopy, these tools require very expensive specialized facilities, high vacuum conditions, and are challenging to scale to large arrays because of the need for custom focus adjustments and drift due to charging effects.[35] The lack of technologies for producing arrays with pores ∼10 nm in turn limits quantitative experiments that can explore the physics of osmotic power generation in these devices, negatively impacting development of practical device designs.

A crucial question is the degree to which high-power densities extrapolated from measurements with single nanopores are truly valid for dense nanopore arrays. A previous experimental and theoretical study[36] performed using 200 nm diameter pores in 50 nm thick membrane silicon nitride (SiN) indicates a sublinear dependence of the pore conductance on the number of the nanopores, N ($G_N = G_{pore}\sqrt{N}$ for 2D nanopore arrays) because of the long-range interaction between the pores. Yet these results were obtained in a different regime where the pore diameter was on the order of the pore spacing and the membrane was not highly charged. Simulation work performed in a thin membrane regime suggests that pore−pore coupling that may limit the achievable power density.[37−39] Yet, these theoretical models made crucial limiting assumptions that prevent extrapolation of the conclusions to real-world systems. For example, the simulations were performed using a 2D planar model that does not account for the complex 3D nature of the ionic transport through the nanopores. Moreover, the simulations may miss additional subtle effects such as diffusio-osmotic flow.[40] There is thus a crucial need for experimental model systems that can quantitatively explore pore coupling phenomena in multipore arrays to complement simulation work and ensure optimum membrane design.

https://doi.org/10.1021/acs.nanolett.0c04704
Nano Lett. 2021, 21, 4152−4159

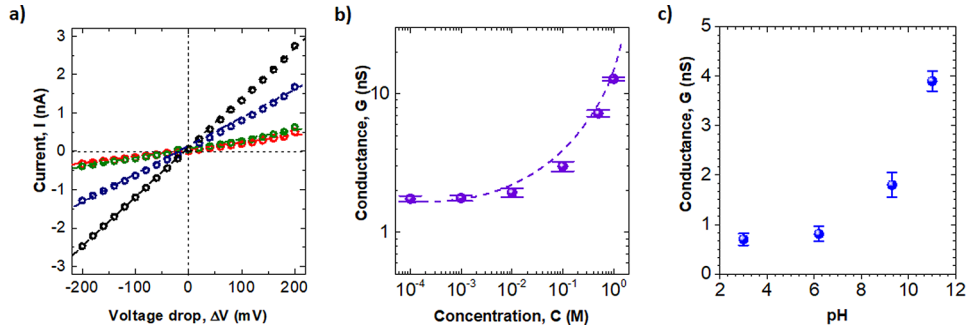

Figure 2. Ionic transport properties and chemical reactivity of a single hBN/SiN nanopore. (a) Current−voltage ($I-V$) measurements (pore diameter: 6 nm, length: 12 nm) at various KCl concentrations (black: 1 M; navy: 10^{-1} M; green: 10^{-2} M, red: 10^{-3} M) at pH = 6. Dashed lines are linear fits from which the conductance $G = I/\Delta V$ is extracted. (b) Conductance vs concentration ($G-C$) for a 6 nm nanopore at pH = 6. The dashed violet line represents the fit using eq 1; the extracted surface charge density (σ_{hBN}) is -0.25 ± 0.04 C·m^{-2}. (c) Conductance as a function of pH at 10^{-3} M KCl concentration for a 5 nm nanopore.

Here we report an approach for scaling of thin membrane nanopore-based osmotic power generation technology from single pore to multipore arrays. We apply our approach to explore how array geometry impacts power-generation performance. In our approach, we coat a sturdy 12 nm thick SiN membrane with a hexagonal boron nitride (hBN) monolayer, remedying the inherent mechanical fragility of the 2D membrane while exploiting hBN's exceptional selectivity arising from its high surface charge (Figure 1). Variable diameter nanopores are then formed in the hBN/SiN membranes using our recently developed nanopore fabrication technique, tip-controlled local breakdown (TCLB).[41,42] TCLB can produce pores sufficiently small (d = 4−16 nm) to achieve optimum selectivity. The nanoscale positioning capability of TCLB then permits the fabrication of pore arrays with a controlled spatial positioning allowing the investigation of multipore systems and pore−pore interaction. We exploit this capability to produce 3 × 3 nanopore arrays with pore-to-pore spacing ranging from ∼100−1000 nm, enabling quantitative testing of the effect of pore density on power output per unit area, a key device performance indicator. Pore conductance measured as a function of electrolyte concentration and pH confirms for our system the dominance of surface conductance over the bulk conductance. Although the thicker hBN/SiN hybrid membranes yield a lower osmotic conductance than suspended hBN, we observed a high osmotic power density that arises from the increased surface charge density on the hBN surface, leading to an enhanced selective ionic transport through nanopores ∼10 nm in diameter. Our work shows that the optimum membrane selectivity and overall power density is obtained with a pore-to-pore spacing of ∼500 nm that balances the need for high pore density while maintaining a large extent of charged surface surrounding each pore.

RESULTS AND DISCUSSION

The hybrid stack membranes were prepared by transferring hBN monolayers grown by chemical vapor deposition (CVD) onto 12 nm thick SiN_x using a polymeric transfer method. Nanopores with 3−16 nm diameters were then drilled in the hBN/SiN stack membranes using TCLB. TCLB allows for fast pore fabrication (≈10 ms/pore) and avoids formation of undesired additional pores on the membranes due to the nanoscale curvature ($r \approx 10$ nm) of the AFM tip that localizes the dielectric breakdown to a nanoscale region. Successful hBN transfer and pore fabrication was confirmed with subsequent SEM, TEM, and AFM imaging (S1-Figures 1 and 2 in Supporting Information).

To gain insight into the surface properties of the hBN/SiN nanopores, we first measured the trans-pore ionic current as a function of electrolyte concentration and pH in the absence of a concentration difference between the reservoirs. Figure 2a shows the linear current−voltage ($I-V$) characteristics of a single hBN/SiN nanopore at various potassium chloride (KCl) concentrations. The dependence of the ionic conductance (G) resulting from these IV measurements ($G = I/\Delta V$) on the electrolyte concentration and pH is shown in Figure 2b,c.

The measured conductance saturates at low salt concentration, a well-known phenomenon reflecting the dominance of counterion driven surface conduction inside the Debye layer. An analytical surface conduction model has been developed by Lee et al.[43] for the nanopore conductance taking in account the additional surface conduction in charged nanopores. Here we introduce a modified analytical model to take into account the hBN coating:

$$G = \kappa_b \left(\frac{4l}{\pi d^2} \frac{1}{1 + \frac{4l_{Du,1}}{d}} + \frac{1}{\alpha d + \beta l_{Du,1}} + \frac{1}{\alpha d + \beta l_{Du,2}} \right)^{-1} \quad (1)$$

The quantity κ_b is the bulk electrolyte conductivity, l is the pore length, d is the pore diameter, α is a geometric prefactor (fixed to 2 as suggested by Hall et al.[44]), and β is a fitting parameter (see Supporting Information S4 for details). The parameter $l_{Du} = \kappa_s/\kappa_b$, termed the Dukhin length, is the length below which surface conductivity (κ_s) dominates the bulk conductivity (κ_b) and is approximated by $\frac{\sigma}{2eC}$ (where σ is the surface conductance, e is the elementary charge, and C is the salt concentration).[43] In this modified surface conduction model, a distinct Dukhin length is introduced in the access resistance corresponding to the upper membrane, $l_{Du,2} = \frac{\sigma_{hBN}}{2eC}$, to account for the enhanced surface charge density of the hBN coated upper membrane surface (σ_{hBN} is the hBN surface charge). This upper membrane Dukhin length is different from the Dukhin length, $l_{Du,1} = \frac{\sigma_{sin}}{2eC}$, corresponding to the uncoated pore interior surfaces and bottom membrane surface (σ_{SiN} is the surface charge of the bare silicon nitride). We have tested the applicability of this model for our hybrid hBN/SiN nanopore by comparing numerical simulations of ion transport through a thin charged nanopore to the modified analytical

https://doi.org/10.1021/acs.nanolett.0c04704
Nano Lett. 2021, 21, 4152−4159

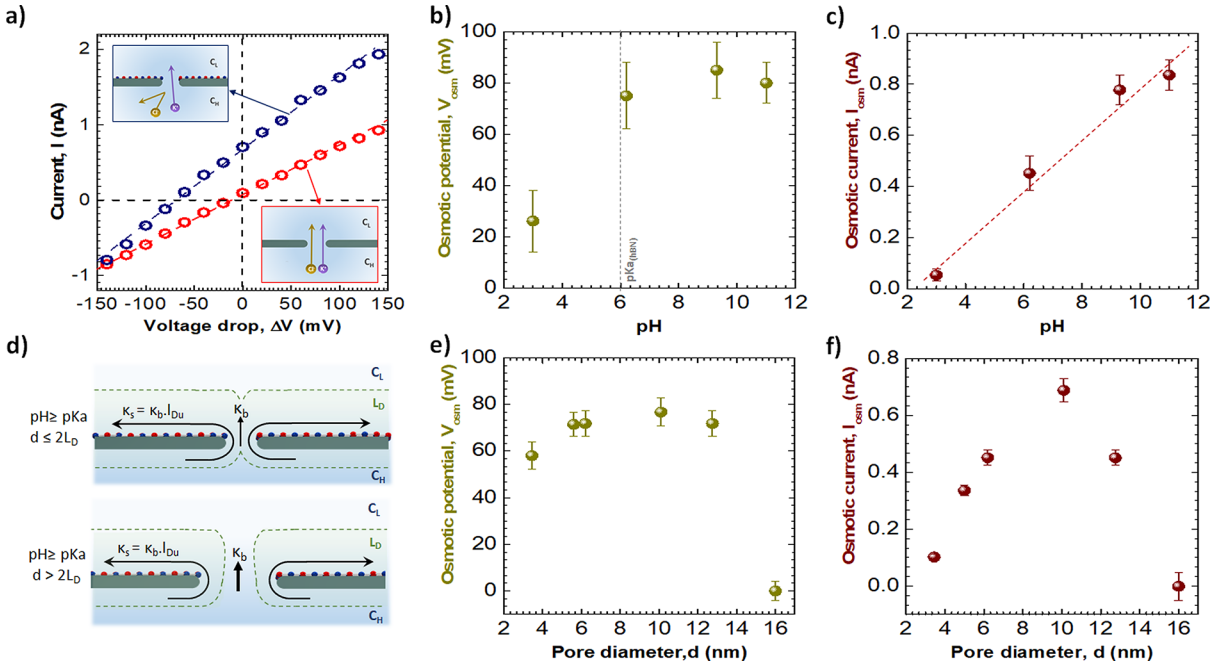

Figure 3. Osmotic power generation in single hBN/SiN nanopore. (a) Current−voltage (I−V) characteristic of hBN/SiN nanopore (blue) and SiN nanopore (red) in a 1 M/1 mM KCl gradient where the hBN layer is on the low KCl concentration side. The insets are a schematic of the hBN/SiN nanopore (left) and SiN nanopore (right); both nanopores are 10 nm in diameter (d) and 12 nm long. The presented data are the pure osmotic contribution after subtracting the contribution of the redox reaction at the electrodes. Osmotic current (I_{osm}) and osmotic potential (V_{osm}) are the y-intercept and x-intercept, respectively. (b) The generated osmotic potential and (c) osmotic current in single 7 nm hBN/SiN as a function of the electrolyte pH. (e) The generated osmotic potential and (f) osmotic current at pH = 6.5 as a function of the nanopore diameter. The same 1 M/1 mM KCl concentration gradient is used for the results in b, c, e, and f. (d) Illustration of the ion transport mechanism through hBN/SiN nanopores (top: pore diameter $d \leq 2L_D$; bottom: $d > L_D$). The highlighted green area represents the Debye layer (L_D) on both sides of the membrane. If $d \leq 2L_D$, the Debye layers overlap at the pore entrance giving rise to selective counterion transport. The two ionic transport pathways: the bulk (κ_b) and the surface (κ_s) conductivity are depicted by the black arrows. The surface-to-bulk conductivity ratio represents the Dukhin length (l_{Du}) over which surface conductance extends.

model (eq 1). In the simulations, σ_{SiN} was fixed while σ_{hBN} was varied. When the modified conductance model (eq 1) is fit to the simulations, we are able to correctly extract the variable upper membrane surface charge that is used as an input parameter in the simulations (see Supporting Information S4-Figure 5).

Equation 1 was then used determine the hBN surface charge. To do this, we first measured the bare silicon nitride surface charge by obtaining a conductance versus concentration curve for an uncoated pore (see Supporting Information S4-Figure 6). Equation 1 was fit to these measurements assuming an identical Dukhin length $l_{Du} = l_{Du,1} = l_{Du,2} = \frac{\sigma_{sin}}{2eC}$ for the lower, upper and interior pore surfaces. The fit yielded a $\sigma_{SiN} = -0.025 \pm 0.001$ C·m^{-2}, comparable to existing literature values.[43] Next, using this value of σ_{SiN}, we fit eq 1 to the conductance versus concentration measurements in Figure 2b for an hBN coated pore, obtaining a value $\sigma_{hBN} = -0.25 \pm 0.04$ C·m^{-2}. The obtained σ_{hBN} is higher than those reported by Siria et al.[45] (i.e., −0.1 C·m^{-2} for a BNNT 15 nm diameter and 800 nm length, at pH = 5)[23] and Weber et al.[46] (i.e., −0.16 C·m^{-2} for a BN nanopore 20 nm diameter and 200 nm long at pH = 7).

Note that the conductance increases with an increase in pH as shown in Figure 2c, suggesting that this charge density can be further enhanced by increasing the electrolyte pH. As reported by Grosjean et al.,[47] the hBN acquires a pH-dependent surface charge density in aqueous medium by hydroxide HO^- adsorption at the boron atoms ($pK_a \approx 6$). The surface charge density is determined by the number of available boron sites on the hBN surface and the solution pH. On the basis of their DFT calculations, Grosjean et al. reported a maximum estimated charge density for hBN ≈ −0.96 C·m^{-2}.

Next, we measure the I−V response of a single nanopore in the presence of a salinity gradient (C_H/C_L = 1000, Figure 3). We chose to place the hBN coated side in contact with the low salinity reservoir. This choice was motivated by the simulation study of Cao et al.[37] that suggests that when one membrane surface has a higher surface charge, such as is the case here due to the hBN coating, the osmotic transport is enhanced when the low-concentration reservoir is placed adjacent to the membrane surface with the higher charge.

The pure osmotic behavior (I_{osm} and V_{osm}) of the nanopore is obtained from the I−V curve after subtracting the electrode Nernst potential contribution (S2 in Supporting Information). The osmotic current (I_{osm}) is the current obtained from the concentration gradient solely at zero applied bias (nonzero y-intercept), while the osmotic potential (V_{osm}) is the voltage required to balance this current (nonzero x-intercept). The maximal power density that can be extracted from the membrane is then obtained from $P_{max} = \frac{1}{4}(I_{osm} \cdot V_{osm})$. As shown in Figure 3a, a large osmotic current and osmotic potential are obtained using a single hBN/SiN nanopore (σ_{hBN} = −0.25 C·m^{-2}), whereas the bare silicon nitride nanopore (σ_{SiN} = −0.025 C·m^{-2}) with the same thickness and pore diameter yields negligible osmotic contribution. The high

https://doi.org/10.1021/acs.nanolett.0c04704
Nano Lett. 2021, 21, 4152−4159

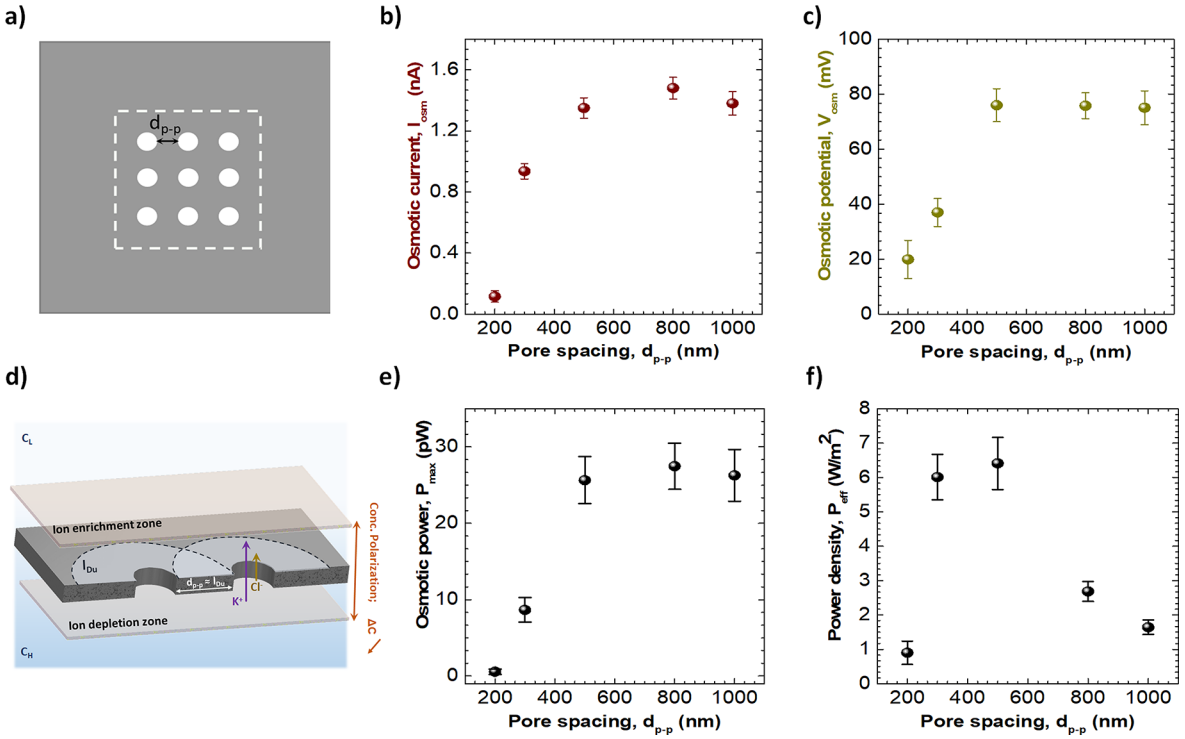

Figure 4. Osmotic power generation in hBN/SiN nanopore arrays. (a) Schematic of the nanopore showing the pore-to-pore spacing d_{p-p}; the dashed square represents the effective area, which is the total area occupied by the array including d_{p-p}^2 about each pore, used for estimating the effective power density. (b) The generated osmotic potential V_{osm}, (c) osmotic current I_{osm}, (e) maximal osmotic power P_{max}, and (f) effective power density P_{eff} for a 3 × 3 nanopore hBN/SiN nanopore array as a function of the pore-to-pore spacing (d_{p-p}). The nanopores used in these measurements have an average 4 nm diameter and are 12 nm long. The measurements were performed in 1 M/1 mM KCl concentration gradient at pH = 6.5. (d) Illustration of a cross sectional view of a nanopore array. The gray shaded area on both sides of the pores represents the area where charge concentration profiles of single nanopores overlap and a strong ion concentration polarization is observed. The dashed shaded semicircle (diameter = $d + l_{Du}$) represents the surface surrounding each pore over which surface conductance extends.

osmotic performance of the hBN/SiN membranes is related to the high ionic selectivity arising from surface charges on the hBN layer. This point is further confirmed by the pH dependence of the osmotic potential which saturates at pH ≤ $pK_{a\ hBN}$ (Figure 3b), revealing that the generation of a net osmotic current and potential in the thin membranes is mainly governed by the hBN surface charge rather than charges on the inner pore surface.

To further probe the mechanism controlling ion selectivity in the hybrid membranes, we explore the effect of membrane charge density and nanopore diameter on the osmotic power generation. The osmotic energy conversion is driven by the chemical potential difference across an ion selective porous membrane. As ions diffuse from the high concentration (C_H) reservoir to the low concentration (C_L) reservoir, a net ionic current (I_{osm}) is generated stemming from the uneven cationic (I^+) and anionic (I^-) fluxes across the membrane; ($I_{osm} = I^+ - I^-$). The origin of the uneven cationic/anionic fluxes can be related to the asymmetric diffusion coefficients of cations (D^+) and anions (D^-) and to the charge separation induced by the charged porous membrane. The asymmetric ionic fluxes lead to the accumulation of cations on one side of the membrane and anions on the other side producing a potential difference across the membrane, that is, V_{osm}, which depends on the membrane ionic selectivity as follows:[8]

$$V_{osm} = S\frac{RT}{zF}\ln\left(\frac{\gamma_H C_H}{\gamma_L C_L}\right) \quad (2)$$

The quantity S is the membrane selectivity (varying from 0 to 1 for nonselective and ideal selective membranes, respectively). The quantities R, T, z, and F are the ideal gas constant, the temperature, the valence number, and the Faraday constant. The quantities γ_H and γ_L are the activity coefficient at high (C_H) and low (C_L) concentration. To explore the contribution of the membrane properties on the I_{osm} and V_{osm}, KCl electrolyte where $D_{K^+} \approx D_{Cl^-}$ was used for all the measurements.

Figure 3c shows a linear increase of osmotic current with pH which can be explained by the increase of membrane charge density ($\sigma = f(\mathrm{pH})$) and Dukhin length ($l_{Du} = \frac{\sigma}{2eC}$), accordingly. The increase in Dukhin length leads to an enhanced apparent electric size ($d_{app} \approx d + l_{Du}$) over which surface conductance extends and thus an enhanced overall conductance and ionic flux (I^+ and I^-). Whereas the osmotic potential tends to saturate at pH ≥ $pK_{a\ hBN}$ (Figure 3b), related to the selectivity mechanism within the hBN/SiN nanopores, the selectivity arises from the electrostatic exclusion of the anions induced by the Debye layer overlap at the pore orifice. Once the hBN surface retains a charge density at pH = pK_a, the selectivity of the membrane ($S = \frac{(I^+ - I^-)}{(I^+ + I^-)}$) increases from ≈0.16 and saturates at ≈0.53 as long as the diameter of the pore remains in the range of the Debye layer overlap ($d \leq 2L_D$, Debye length (L_D) ≈ 10 nm for 1 mM KCl) independent of the surface charge density.

https://doi.org/10.1021/acs.nanolett.0c04704
Nano Lett. 2021, 21, 4152−4159

A similar effect is observed for I_{osm} and V_{osm} as a function of pore diameters (Figure 3e,f). For smaller pores ($d \leq 2L_D$), the selectivity and thus V_{osm} are retained at ≈0.53 due to the L_D overlap while I_{osm} increases as the pore diameter is increased. A sudden drop is then observed for both V_{osm} and I_{osm} at large nanopore diameters (d > 10 nm) once the electrostatic exclusion of anions and the uneven ionic diffusion is lost. In a thin membrane, as the pore diameter increases, the lack of Debye layer overlap at the high concentration side will degrade the electrostatic selectivity of the nanopore even in the presence of Debye layer overlap at low concentration side. This can be explained by ions leaking into the pore from the high concentration entrance preventing the Debye overlap throughout the entire pore body. Cao L.et al.[37] reported that the membrane potential of a 2 nm long nanopore declines by 88% when the pore diameter increases from 2 to 20 nm. Accordingly, the pore selectivity is likely related to the aspect ratio of the pore (L/D). As the aspect ratio of the pore drops below 1, the selectivity will be worsened by the high concentration gradient. Because of the thicker membranes used in our study (12 nm thick), the selectivity is retained up to a 10 nm diameter (L/D = 1.2).

The results obtained with single nanopore systems highlight the importance of the surrounding charged surface and the nanopore diameter on the unique performance of the hBN/SiN nanopores. However, the viability of employing a hBN/SiN power generator largely depends on the possibility of producing large scale nanopore arrays with high power densities per unit area. Employing the precise positioning of the TCLB technique, 2D nanopore arrays with precisely controlled pore-to-pore spacing (d_{p-p}) varying from 100 nm to 1 μm are fabricated (Figure 4a), and their power generation performance was tested using KCl electrolyte under a salinity gradient (C_H/C_L = 1000). A nonlinear growth of the osmotic current and potential with increasing interpore distance is observed (Figure 4b,c), leading to growth in the osmotic power generated (Figure 4e), suggesting that a critical charged region surrounding the nanopore is required to sustain the power generation efficiency of hBN/SiN nanopores. Figure 4e suggest this region is ∼500 nm, which is smaller than the values reported by Cao et al.[37] (i.e., ∼1000 nm). With an interpore distance shorter than 500 nm, the pore−pore interactions become significant and the osmotic performance of the membrane is compromised.

The critical pore-to-pore spacing required to sustain high power generation is a crucial design parameter. Since the surface conductance extends over Dukhin length (l_{Du}) outside the pore, a decrease in the overall conductance and thus osmotic current (I_{osm}) will be observed when the pore-to-pore spacing becomes comparable to l_{Du}. The Dukhin length corresponding to the hBN coated upper membrane is 1.3 ± 0.2 μm (Figure 4d, at 1 mM KCl electrolyte on hBN side considering 0.25 C·m^{-2} nanopore surface charge density). In addition, a strong ion concentration polarization will occur originating from the increased pore density and the overlap of charge concentration clouds associated with nanopores in the array. This concentration polarization induces a depletion of the local concentration gradient (C_H/C_L) across the nanopore array resulting in a reduction of the osmotic transport (I_{osm} and V_{osm}) through the nanopores. An interplay likely exists between the Dukhin length and the concentration polarization effect that leads to the critical pore-to-pore spacing at which the power generation efficiency is reduced, but further work is needed to clarify the physical origins of this critical length scale. We note that our critical pore-to-pore spacing is lower than the Dukhin length for the hBN coated surface by about a factor of 2. In Cao et al., the critical pore-to-pore spacing they observe is around 1 μm, which is higher than their Dukhin length (0.3 μm at the low concentration side).

The key indicator of the power generation potential of our array is the maximum effective power density P_{eff}, defined as P_{max} divided by the effective array area (Figure 4f). The maximum effective power density takes into account the combined effects of pore-to-pore coupling and the effect of simply varying the number of power generating pores per unit area. Pore-to-pore coupling decreases the power generated for low pore-to-pore spacing; decreasing the number of power generating pores available per unit area decreases the power at high pore-to-pore spacing. The result is a maximum effective power density output at a pore-to-pore spacing that balances these two effects; our measurements suggest this maximum occurs at a pore−pore spacing of ≈500 nm. Thus, optimum extrapolation of single nanopore power generators to multipore arrays necessitate that a fixed charged area surround each pore with a radius of ≈500 nm. The maximum obtained power density ≈15 W·m^{-2} in our study was obtained using a 3 × 3 array with nanopores of ≈6 nm in diameter and 500 nm pore-to-pore spacing at pH = 6.5 (Figure 4c in Supporting Information). This can be translated into 0.3 MWm^{-2} (per pore unit surface) for a single hBN/SiN nanopore in the array, just under the values obtained with suspended single layer MoS_2 membranes (1 MWm^{-2} per pore area, for a 10 nm pore at pH = 11).

Lastly, while we have demonstrated production of 3 × 3 pore arrays, TCLB can be scaled to produce much larger arrays. We have demonstrated a 20 × 20 pore array on a 40 × 40 μm^2 area (S1-Figure 3). This array, produced with a 25 min writing time, gives a write time of around 16 pores/min (dominated by tip translation time, pore fabrication time ∼ ms). Higher throughput could potentially be achieved with AFM scanning cantilevers designed for parallel scanning that can incorporate 4096 tips.[48]

CONCLUSION

Here we have developed a nanopore embedded hybrid hBN/SiN based membrane for osmotic power generation. The high osmotic transport obtained using these membranes appears to originate from the charge separation in the Debye layer formed on the outer charged membrane around the nanopore. Since the surface charges on the outer membrane are the main contributor to the transport mechanism, combining fragile highly charged 2D materials with mechanically stable thin membranes, SiN for instance, resolves the inherent mechanical stability issues of using monolayer hBN while allowing exploitation of hBN's high surface charge. In addition, our approach exploits TCLB to scale from single pores to multipore arrays. TCLB can construct arrays of pores ∼10 nm in diameter with controlled spacings. Exploiting TCLB's ability to control array geometry, we quantitatively explore how the array power output per unit area scales with pore spacing. We find that the power output is extremely sensitive to pore-to-pore spacing, as suggested by recent theory. We attribute this sensitivity to the long-range nature of the transport mechanism originating from the surface conductance extending over the Dukhin length and the overlap of the concentration profiles of neighboring nanopores in densely

https://doi.org/10.1021/acs.nanolett.0c04704
Nano Lett. 2021, 21, 4152−4159

packed nanoporous arrays that compromise the osmotic transport across the membrane. In the future, given our ability to control array geometry, our experimental model could be extended to explore the effect of other features that might compromise performance of real-world systems, for example, inhomogeneous pore size and pore spacing.

■ ASSOCIATED CONTENT

Supporting Information

The Supporting Information is available free of charge at https://pubs.acs.org/doi/10.1021/acs.nanolett.0c04704.

S1: AFM scans, SEM and TEM images of the transferred hBN monolayer onto SiN membranes, and TEM images of the drilled nanopores; S2: experimental setup, S3: control experiments and normalization of power generation data; and S4: ionic conductance modeling (PDF)

■ AUTHOR INFORMATION

Corresponding Authors

Peter Grutter − *Department of Physics, McGill University, Montreal, Quebec H3A 2T8, Canada;* orcid.org/0000-0003-1719-8239; Email: peter.grutter@mcgill.ca

Walter W. Reisner − *Department of Physics, McGill University, Montreal, Quebec H3A 2T8, Canada;* orcid.org/0000-0003-3223-615X; Email: reisner@physics.mcgill.ca

Authors

Khadija Yazda − *Department of Physics, McGill University, Montreal, Quebec H3A 2T8, Canada;* orcid.org/0000-0001-6010-1776

Katarina Bleau − *Department of Physics, McGill University, Montreal, Quebec H3A 2T8, Canada*

Yuning Zhang − *Department of Physics, McGill University, Montreal, Quebec H3A 2T8, Canada; BGI-Shenzhen, Shenzhen 518083, China*

Xavier Capaldi − *Department of Physics, McGill University, Montreal, Quebec H3A 2T8, Canada;* orcid.org/0000-0002-0396-3510

Thomas St-Denis − *Department of Physics, McGill University, Montreal, Quebec H3A 2T8, Canada*

Complete contact information is available at: https://pubs.acs.org/10.1021/acs.nanolett.0c04704

Funding

Financial support for this work was provided by the McGill Sustainability Systems Initiative (MSSI) Ideas Fund (172584), Natural Sciences and Engineering Research Council of Canada (NSERC), Discovery Grants Program (Grant No. RGPIN-2016-05033 and RGPIN-2018-06125), and RQMP funded by FRQ-NT.

Notes

The authors declare no competing financial interest.

■ ACKNOWLEDGMENTS

The authors acknowledge Norcada for material supplies (silicon nitride membranes) and acknowledge H. Hosseinkhannazer and M. Safari for useful discussions. The authors acknowldge Dr. V. Jourdain for his helpful comments on the manuscript. The authors acknowledge Facility for Electron Microscopy Research (FEMR) at McGill for access to electron microscope.The authors acknowledge J.P. Masse at Centre de Caractérisation Microscopique des Matériaux $(CM)^2$ at Ecole Polytechnique de Montréal for Transmission electron microscoy characterizations.

■ REFERENCES

(1) White, B. E. Energy-harvesting devices: Beyond the battery. *Nat. Nanotechnol.* **2008**, *3*, 71−72.

(2) Baxter, J.; et al. Nanoscale design to enable the revolution in renewable energy. *Energy Environ. Sci.* **2009**, *2*, 559−588.

(3) Pennathur, S.; Eijkel, J. C.; Van Den Berg, A. Energy conversion in microsystems: Is there a role for micro/nanofluidics? *Lab Chip* **2007**, *7*, 1234−1237.

(4) Siddique, A. R. M.; Mahmud, S.; Heyst, B. V. A comprehensive review on vibration based micro power generators using electromagnetic and piezoelectric transducer mechanisms. *Energy Convers. Manage.* **2015**, *106*, 728−747.

(5) Yang, R.; Qin, Y.; Li, C.; Zhu, G.; Wang, Z. L. Converting Biomechanical Energy into Electricity by a Muscle-Movement-Driven Nanogenerator. *Nano Lett.* **2009**, *9*, 1201−1205.

(6) Li, K.; He, Q.; Wang, J.; Zhou, Z.; Li, X. Wearable energy harvesters generating electricity from low-frequency human limb movement. *Microsystems and Nanoengineering* **2018**, *4*, 24.

(7) Yan, J.; Liao, X.; Yan, D.; Chen, Y. Review of Micro Thermoelectric Generator. *J. Microelectromech. Syst.* **2018**, *27*, 1−18.

(8) Kim, D. K.; Duan, C.; Chen, Y. F.; Majumdar, A. Power generation from concentration gradient by reverse electrodialysis in ion-selective nanochannels. *Microfluid. Nanofluid.* **2010**, *9*, 1215−1224.

(9) Guo, W.; Cao, L.; Xia, J.; Nie, F. Q.; Ma, W.; Xue, J.; Song, Y.; Zhu, D.; Wang, Y.; Jiang, L. Energy harvesting with single-ion-selective nanopores: A concentration-gradient-driven nanofluidic power source. *Adv. Funct. Mater.* **2010**, *20*, 1339−1344.

(10) Pattle, R. E. Production of electric power by mixing fresh and salt water in the hydroelectric pile. *Nature* **1954**, *174*, 660.

(11) Chou, S.; Wang, R.; Shi, L.; She, Q.; Tang, C.; Fane, A. G. Thin-film composite hollow fiber membranes for pressure retarded osmosis (PRO) process with high power density. *J. Membr. Sci.* **2012**, *389*, 25−33.

(12) Post, J. W.; Veerman, J.; Hamelers, H. V.; Euverink, G. J.; Metz, S. J.; Nymeijer, K.; Buisman, C. J. Salinity-gradient power: Evaluation of pressure-retarded osmosis and reverse electrodialysis. *J. Membr. Sci.* **2007**, *288*, 218−230.

(13) Veerman, J.; Saakes, M.; Metz, S. J.; Harmsen, G. J. Electrical power from sea and river water by reverse electrodialysis: A first step from the laboratory to a real power plant. *Environ. Sci. Technol.* **2010**, *44*, 9207−9212.

(14) Chang, C.-R.; Yeh, C.-H.; Yeh, H.-C.; Yang, R.-J. Energy Conversion From Salinity Gradient Using Microchip With Nafion Membrane. *Int. J. Mod. Phys.: Conf. Ser.* **2016**, *42*, 1660183.

(15) Catalano, J.; Bentien, A. Influence of temperature on the electrokinetic properties and power generation efficiency of Nafion® 117 membranes. *J. Power Sources* **2014**, *262*, 192−200.

(16) Hsu, J. P.; Lin, S. C.; Lin, C. Y.; Tseng, S. Power generation by a pH-regulated conical nanopore through reverse electrodialysis. *J. Power Sources* **2017**, *366*, 169−177.

(17) De Vreede, L. J.; Van Den Berg, A.; Eijkel, J. C. Nanopore fabrication by heating au particles on ceramic substrates. *Nano Lett.* **2015**, *15*, 727−731.

(18) Tong, H. D.; Jansen, H. V.; Gadgil, V. J.; Bostan, C. G.; Berenschot, E.; Van Rijn, C. J.; Elwenspoek, M. Silicon Nitride Nanosieve Membrane. *Nano Lett.* **2004**, *4*, 283−287.

(19) Dai, J.; Singh, J.; Yamamoto, N. Nonbrittle nanopore deformation of anodic aluminum oxide membranes. *J. Am. Ceram. Soc.* **2018**, *101*, 2170−2180.

(20) Lee, S. W.; Kim, H. J.; Kim, D. K. Power generation from concentration gradient by reverse electrodialysis in dense silica

membranes for microfluidic and nanofluidic systems. *Energies* **2016**, *9*, 49.
(21) Yan, F.; Yao, L.; Chen, K.; Yang, Q.; Su, B. An ultrathin and highly porous silica nanochannel membrane: Toward highly efficient salinity energy conversion. *J. Mater. Chem. A* **2019**, *7*, 2385−2391.
(22) Kalra, A.; Garde, S.; Hummer, G. (CUL-ID:1887995) From The Cover: Osmotic water transport through carbon nanotube membranes. *Proc. Natl. Acad. Sci. U. S. A.* **2003**, *100*, 10175−10180.
(23) Siria, A.; Poncharal, P.; Biance, A. L.; Fulcrand, R.; Blase, X.; Purcell, S. T.; Bocquet, L. Giant osmotic energy conversion measured in a single transmembrane boron nitride nanotube. *Nature* **2013**, *494*, 455−458.
(24) Rollings, R.; Kuan, A.; Golovchenko, J. Ion selectivity of graphene nanopores. *Nat. Commun.* **2016**, *7*, 11408.
(25) Cohen-Tanugi, D.; Grossman, J. C. Nanoporous graphene as a reverse osmosis membrane: Recent insights from theory and simulation. *Desalination* **2015**, *366*, 59−70.
(26) Homaeigohar, S.; Elbahri, M. Graphene membranes for water desalination. *NPG Asia Mater.* **2017**, *9*, e427−e427.
(27) Walker, M. I.; Ubych, K.; Saraswat, V.; Chalklen, E. A.; Braeuninger-Weimer, P.; Caneva, S.; Weatherup, R. S.; Hofmann, S.; Keyser, U. F. Extrinsic Cation Selectivity of 2D Membranes. *ACS Nano* **2017**, *11*, 1340−1346.
(28) Feng, J.; Graf, M.; Liu, K.; Ovchinnikov, D.; Dumcenco, D.; Heiranian, M.; Nandigana, V.; Aluru, N. R.; Kis, A.; Radenovic, A. Single-layer MoS2 nanopores as nanopower generators. *Nature* **2016**, *536*, 197−200.
(29) Huang, Z.; Zhang, Y.; Hayashida, T.; Ji, Z.; He, Y.; Tsutsui, M.; Miao, X. S.; Taniguchi, M. The impact of membrane surface charges on the ion transport in MoS2 nanopore power generators. *Appl. Phys. Lett.* **2017**, *111*, 263104.
(30) Graf, M.; Lihter, M.; Unuchek, D.; Sarathy, A.; Leburton, J. P.; Kis, A.; Radenovic, A. Light-Enhanced Blue Energy Generation Using MoS2 Nanopores. *Joule* **2019**, *3*, 1549−1564.
(31) Macha, M.; Marion, S.; Nandigana, V. V. R.; Radenovic, A. 2D materials as an emerging platform for nanopore-based power generation. *Nature Reviews Materials* **2019**, *4*, 588−605.
(32) Zhang, R.; Cheung, R. In *Mechanical Properties and Applications of Two-Dimensional Materials, Two-dimensional Materials - Synthesis, Characterization and Potential Applications*; Nayak, P. K., Ed.; IntechOpen, 2016.
(33) Feng, J.; Liu, K.; Graf, M.; Lihter, M.; Bulushev, R.; Dumcenco, D.; Alexander, D.; Krasnozhon, D.; Vuletic, T.; Kis, A.; Radenovic, A. Electrochemical Reaction in Single Layer MoS2: Nanopores Opened Atom by Atom. *Nano Lett.* **2015**, *15*, 3431−8.
(34) Kwok, H.; Briggs, K.; Tabard-Cossa, V. Nanopore Fabrication of Two-Dimensional Materials on SiO2Membranes Using He Ion Microscopy. *PLoS One* **2014**, *9*, e92880.
(35) Hayashi, T.; Arima, K.; Yamashita, N.; Park, S.; Ma, Z.; Tabata, O.; Kawai, K. Nanopore Fabrication by Controlled Dielectric Breakdown. *IEEE Trans. Nanotechnol.* **2018**, *17*, 727−730.
(36) Gadaleta, A.; Sempere, C.; Gravelle, S.; Siria, A.; Fulcrand, R.; Ybert, C.; Bocquet, L. Sub-additive ionic transport across arrays of solid-state nanopores. *Phys. Fluids* **2014**, *26*, 012005.
(37) Cao, L.; Wen, Q.; Feng, Y.; Ji, D.; Li, H.; Li, N.; Jiang, L.; Guo, W. On the Origin of Ion Selectivity in Ultrathin Nanopores: Insights for Membrane-Scale Osmotic Energy Conversion. *Adv. Funct. Mater.* **2018**, *28*, 1804189.
(38) Gao, J.; Liu, X.; Jiang, Y.; Ding, L.; Jiang, L.; Guo, W. Understanding the Giant Gap between Single-Pore- and Membrane-Based Nanofluidic Osmotic Power Generators. *Small* **2019**, *15*, 1804279.
(39) Xiao, F.; Ji, D.; Li, H.; Tang, J.; Feng, Y.; Ding, L.; Cao, L.; Li, N.; Jiang, L.; Guo, W. A general strategy to simulate osmotic energy conversion in multi-pore nanofluidic systemsâ€. *Materials Chemistry Frontiers* **2018**, *2*, 935−941.
(40) Yoshida, H.; Marbach, S.; Bocquet, L. Osmotic and diffusio-osmotic flow generation at high solute concentration. II. Molecular dynamics simulations. *J. Chem. Phys.* **2017**, *146*, 194702.
(41) Zhang, Y.; Miyahara, Y.; Derriche, N.; Yang, W.; Yazda, K.; Capaldi, X.; Liu, Z.; Grutter, P.; Reisner, W. Nanopore Formation via Tip-Controlled Local Breakdown Using an Atomic Force Microscope. *Small Methods* **2019**, *3*, 1900147.
(42) St-Denis, T.; Yazda, K.; Capaldi, X.; Bustamante, J.; Safari, M.; Miyahara, Y.; Zhang, Y.; Grutter, P.; Reisner, W. An apparatus based on an atomic force microscope for implementing tip-controlled local breakdown. *Rev. Sci. Instrum.* **2019**, *90*, 123703.
(43) Lee, C.; Joly, L.; Siria, A.; Biance, A. L.; Fulcrand, R.; Bocquet, L. Large apparent electric size of solid-state nanopores due to spatially extended surface conduction. *Nano Lett.* **2012**, *12*, 4037−4044.
(44) Hall, J. E. Access resistance of a small circular pore. *J. Gen Physiol* **1975**, *66*, 531−532.
(45) Siria, A.; Poncharal, P.; Biance, A. L.; Fulcrand, R.; Blase, X.; Purcell, S. T.; Bocquet, L. Giant osmotic energy conversion measured in a single transmembrane boron nitride nanotube. *Nature* **2013**, *494*, 455−458.
(46) Weber, M.; Koonkaew, B.; Balme, S.; Utke, I.; Picaud, F.; Iatsunskyi, I.; Coy, E.; Miele, P.; Bechelany, M. Boron Nitride Nanoporous Membranes with High Surface Charge by Atomic Layer Deposition. *ACS Appl. Mater. Interfaces* **2017**, *9*, 16669−16678.
(47) Grosjean, B.; Pean, C.; Siria, A.; Bocquet, L.; Vuilleumier, R.; Bocquet, M. L. Chemisorption of Hydroxide on 2D Materials from DFT Calculations: Graphene versus Hexagonal Boron Nitride. *J. Phys. Chem. Lett.* **2016**, *7*, 4695−4700.
(48) Eleftheriou, E.; Antonakopoulos, T.; Binnig, G. K.; Cherubini, G.; Despont, M.; Dholakia, A.; Durig, U.; Lantz, M. A.; Pozidis, H.; Rothuizen, H.; Vettiger, P. "Millipede": a MEMS-based scanning-probe data-storage system. *IEEE Trans. Magn.* **2003**, *39*, 938−945.

https://doi.org/10.1021/acs.nanolett.0c04704
Nano Lett. 2021, 21, 4152−4159